GRIFFITH UNIVERSITY

Chaotic properties of isokinetic-isobaric atomic systems under planar shear and elongational flows

Author

Frascoli, Federico, Bernhardt, Debra, Todd, B.

Published

2008

Journal Title

Physical Review E (Statistical, Nonlinear, and Soft Matter Physics)

DOI

10.1103/PhysRevE.77.056217

Rights statement

© 2008 American Physical Society. This is the author-manuscript version of this paper. Reproduced in accordance with the copyright policy of the publisher. Please refer to the journal link for access to the definitive, published version.

Downloaded from

http://hdl.handle.net/10072/21776

Link to published version

http://pre.aps.org/

Griffith Research Online

https://research-repository.griffith.edu.au

Chaotic properties of isokinetic-isobaric atomic systems under planar shear and elongational flows

Federico Frascoli[1], Debra J. Searles[2] and B. D. Todd[3]

[1, 3]*Centre for Molecular Simulation, Swinburne University of Technology, PO Box 218, Hawthorn, Victoria 3122, Australia*

[2]*Nanoscale Science and Technology Centre, School of Biomolecular and Physical Sciences, Griffith University, Brisbane QLD 4111, Australia*

Abstract

An investigation of the chaotic properties of nonequilibrium atomic systems under planar shear and planar elongational flows is carried out for a constant pressure and temperature ensemble, with the combined use of a Gaussian thermostat and a Nosé-Hoover integral feedback mechanism for pressure conservation. A comparison with Lyapunov spectra of atomic systems under the same flows and at constant volume and temperature shows that, regardless of whether the underlying algorithm describing the flow is symplectic, the degrees of freedom associated with the barostat have no overall influence on chaoticity and the general conjugate pairing properties are independent of the ensemble. Finally, the dimension of the strange attractor onto which the phase space collapses is found not to be significantly altered by the presence of the Nosé-Hoover barostatting mechanism.

[1] ffrascoli@swin.edu.au
[2] D.Bernhardt@griffith.edu.au
[3] btodd@swin.edu.au

1. Introduction

The chaotic properties of atomic liquid systems in a nonequilibrium steady state have been extensively studied in the last two decades [1-11]. In general, one of the most widely accepted requirements for a system to be chaotic is that it must have at least one positive Lyapunov exponent, which is a measure of the mean exponential rate of expansion and contraction of initially nearby phase space trajectories. The Lyapunov spectra for different field-driven systems out of equilibrium have been computed for a number of interesting nonequilibrium molecular dynamics [12, 13] (NEMD) models and one of the most significant developments has been the establishment of a fundamental link between Lyapunov exponents and transport coefficients [9, 14].

In this study, we present the Lyapunov spectra for nonequilibrium steady state systems of simple atoms interacting via a pairwise additive Weeks-Chandler-Anderson (WCA) potential [15] and subjected either to PSF or PEF, in a constant temperature and pressure (*NpT*) ensemble. This is sampled with the adoption of a Gaussian isokinetic mechanism for instantaneous conservation of temperature [12] combined with a Nosé-Hoover (NH) barostatting mechanism for constant pressure [16]. For shear, we simulate a planar Couette flow system via the well-established non-Hamiltonian SLLOD algorithm and Lees-Edwards periodic boundary conditions (pbcs) [12]. For elongation, we employ the Hamiltonian SLLOD algorithm for PEF with “deforming-brick” pbcs [17-20] and use an Arnold cat map

scheme [21] to impose the periodicity relations on the unit lattice. The cat map was recently shown [22] to be related to the Kraynik-Reinelt (KR) conditions [23] for the compatibility and reproducibility of the simulation box, which are necessary requirements for the fundamental cell in order to have indefinitely long PEF simulations.

As observed in a previous study [7], Lyapunov spectra of PEF systems at *NVT* (i.e. at constant volume and temperature) and *NVE* (i.e. at constant volume and energy) satisfy the so-called Conjugate Pairing Rule (CPR) [24, 25]. CPR implies an equal sum for all the Lyapunov pairs in the spectrum, formed by coupling the highest exponent with the lowest, the second highest with the second lowest, and so on. Whereas for elongation the CPR compliance is essentially due to its symplectic character, conjugate pairing was observed to be violated by SLLOD PSF at both *NVT* and *NVE*, in accordance with preceding numerical calculations [6] and theoretical arguments [26, 27]. As repeatedly stressed in the literature, the satisfaction of CPR is not only important *per se*, but it leads to a dramatic reduction in the amount of calculation required to compute the dynamical properties of the system related to the sum of the exponents.

The paper is organized as follows: in Section 2 the features of PSF and PEF and their algorithms at *NpT* are explained, briefly illustrating the characteristics of the NH barostatting procedure, and discussing the method for the calculation of Lyapunov exponents and their main properties. After describing the quantities of interest for our set of simulations in Section 3, a presentation of Lyapunov spectra

at *NpT* for nonequilibrium systems of 8 particles is carried out in Section 4. Here we propose a comparison with analogous results at constant volume and temperature, and analyze the properties of those exponents associated with the NH degrees of freedom at a number of different state points. Some final remarks and an Appendix, where explicit calculations of the Jacobian of the system are shown, conclude the paper.

2. Description of the model

Using nonequilibrium molecular dynamics methods, we simulate a 2 dimensional system of 8 atoms subject to PSF and PEF in an *NpT* thermodynamic ensemble, which is realized with the combined use of a Gaussian isokinetic thermostat and a Nosé-Hoover barostatting mechanism [16]. The atoms interact via the WCA potential [15], which is a truncated and shifted version of the Lennard-Jones potential:

$$\phi(r_{ij})=\begin{cases} 4\varepsilon\left[\left(\frac{\sigma}{r_{ij}}\right)^{12}-\left(\frac{\sigma}{r_{ij}}\right)^{6}\right]+\phi_{\mathrm{c}} & \text{for } r_{ij} < r_c \\ 0 & \text{for } r_{ij} > r_c \end{cases} \tag{1}$$

with $r_{ij}=\left|\mathbf{q}_i-\mathbf{q}_j\right|$, where $\mathbf{q}_i$ is the laboratory position vector of particle *i*, ε is the well depth and σ is the value at which the Lennard-Jones potential is zero. ϕ_c is the

value of the unshifted potential at the cut off distance $r_c = 2^{1/6}\sigma$, so that the WCA potential is continuous. In the following we use reduced units, set all the masses of the particles m_i to be equal to m, and impose $m = \sigma = \varepsilon = 1$.

It is convenient to write SLLOD equations for shear and elongation coupled with a Nosé-Hoover barostat using reduced coordinates $\mathbf{r}_i = \mathbf{q}_i / V^{1/d}$ [16], where V and $d = 2$ are the volume and the dimensionality of the system, respectively. The equations of motion for the reduced laboratory positions $\mathbf{r}_i$ and the peculiar momenta $\mathbf{p}_i$ of a system of simple atoms under PSF, with streaming velocity in the x-direction and gradient in the y-direction, are given by [12]

$$\begin{aligned} \dot{\mathbf{r}}_i &= \frac{\mathbf{p}_i}{mV^{1/d}} + \mathbf{i}\dot{\gamma} y_i \\ \dot{\mathbf{p}}_i &= \mathbf{F}_i - \mathbf{i}\dot{\gamma} p_{yi} - \alpha_{PSF}\mathbf{p}_i \end{aligned} \tag{2}$$

and the Gaussian isokinetic multiplier, which ensures that the kinetic energy is fixed at all times, is represented by

$$\alpha_{PSF} = \frac{\sum_{i=1}^{N} \mathbf{F}_i \cdot \mathbf{p}_i - \dot{\gamma} p_{xi} p_{yi}}{\sum_{i=1}^{N} \mathbf{p}_i \cdot \mathbf{p}_i} \tag{3}$$

The peculiar momentum is defined as the one taken with respect to the streaming momentum $m\mathbf{u}$, $\mathbf{i}$ is the unit vector in the x direction, $\mathbf{F}_i$ is the total interatomic force acting on particle i, and $\dot{\gamma} = \partial u_x / \partial y$ is the shear rate. Similarly, for a system under PEF, with expansion in the x direction and contraction in the y direction, the equations are [17]

$$\begin{aligned}\dot{\mathbf{r}}_i &= \frac{\mathbf{p}_i}{mV^{1/d}} + \dot{\varepsilon}\left(\mathbf{i}x_i - \mathbf{j}y_i\right) \\ \dot{\mathbf{p}}_i &= \mathbf{F}_i - \dot{\varepsilon}\left(\mathbf{i}p_{xi} - \mathbf{j}p_{yi}\right) - \alpha_{PEF}\mathbf{p}_i\end{aligned} \tag{4}$$

and the Gaussian thermostat multiplier has the form

$$\alpha_{PEF} = \frac{\sum_{i=1}^{N} \mathbf{F}_i \cdot \mathbf{p}_i - \dot{\varepsilon}\left(p_{xi}^2 - p_{yi}^2\right)}{\sum_{i=1}^{N} \mathbf{p}_i \cdot \mathbf{p}_i} \tag{5}$$

where $\mathbf{j}$ is the unit vector in the *y* direction and $\dot{\varepsilon} = \partial u_x / \partial x = -\partial u_y / \partial y$ is the elongational rate.

Expressions (2)-(5) have to be complemented with the differential equations that describe the NH mechanism for pressure conservation, which introduces two additional degrees of freedom in the system: the volume *V* of the simulation cell and an external variable, $\dot{\xi}$, that mimics a piston [28]. The time evolution of *V* is regulated by $\dot{\xi}$ via the following equation:

$$\dot{V} = d\dot{\xi}V \tag{6}$$

where $\dot{V}$ is the first derivative of the cell volume with respect to time. Likewise, $\dot{\xi}$ is the solution of the following differential equation:

$$\ddot{\xi} = \frac{\left(p - p_0\right)V}{Nk_BTQ} \tag{7}$$

In the last formula, *p* is the instantaneous pressure of the system, given as the trace of the pressure tensor

$$\mathbf{P} = \frac{1}{V}\left(\sum_{i=1}^{N} \frac{\mathbf{p}_i \mathbf{p}_i}{m} + \sum_{i=1}^{N} \sum_{j>i}^{N} \left(\mathbf{q}_i - \mathbf{q}_j \right) \mathbf{F}_{ij} \right) \tag{8}$$

divided by the dimensionality d, p_0 is the target pressure and N is the number of atoms. Q is a damping factor which is chosen by trial and error so that pressure fluctuations are appropriately reduced, as described in [29, 30], and $\mathbf{F}_{ij} = -\partial \phi_{ij} / \partial \mathbf{q}_i$ is the force on particle i due to particle j. It should be noted that Eqs. (2)-(5) do not explicitly contain $\dot{\xi}$, as it has been absorbed in the derivative of the reduced positions $\dot{\mathbf{r}}_i$ via Eq. (6), and that the force terms appearing in (2), (4) and (8) are calculated from a WCA potential which depends on the unscaled distances among the particles.

As it is customary in NEMD [19], pbcs have to be imposed on the simulation cell to preserve the homogeneity of the sample, eliminate surface effects and allow the system to reach a steady state [12]. For PSF, Lees-Edwards pbcs [31] are employed in a straightforward way in conjunction with Eqs. (6)-(7) that regulate pressure conservation. Since under this scheme image cells are only shifted along the direction of the flow [19], the target pressure p_0 is achieved and maintained by a periodic rescaling of each boxlength, so that the volume of the unit cell is equal to the target volume solution of Eq. (6). On the other hand, Kraynik-Reinelt pbcs have been shown to be necessary for performing homogeneous simulations of steady planar elongation for indefinitely long times [17, 18, 22, 23]. These conditions imply that the fundamental cell contracts and expands as time evolves, and care must be taken in the rescaling of the cell to ensure that the *NpT* PEF ensemble is

correctly sampled. A procedure for this, which implements a method known as the "new-cell algorithm" in combination with deforming bricks pbcs [18], has been fully described in [30]. It has also been shown that, for SLLOD PEF, Lyapunov instability causes the *y* component of the total momentum to drift, due to numerical roundoff errors, more substantially in PEF than in equilibrium or PSF simulations, and therefore we reset it at each timestep [32]. This procedure has no effect on the properties that are calculated.

There is one exponent for each degree of freedom in the system. The computation of the spectrum of Lyapunov exponents is performed with the well-established algorithm by Benettin *et al.* [33-36]. In short, consider a vector $\mathbf{\Gamma}_1(t) = \left[\mathbf{r}(t),\ \mathbf{p}(t),\ V(t),\ \dot{\xi}(t) \right]$ in the extended phase-space comprising the two extra Nosé-Hoover degrees of freedom, and a displacement $\delta\mathbf{\Gamma}_n(t) = \mathbf{\Gamma}_1(t) - \mathbf{\Gamma}_n(t)$ whose evolution can be expressed to first order by $\delta\dot{\mathbf{\Gamma}}(t) = \mathbf{T}(t) \cdot \delta\mathbf{\Gamma}(t)$. $\mathbf{T}$ is the stability matrix or the Jacobian of the equations of motion, and the explicit calculation of its elements for a *NpT* system is illustrated in the Appendix. We can define a set of orthogonal vectors $\delta\mathbf{\Gamma}_n^c$, such that $\delta\mathbf{\Gamma}_n^c \cdot \delta\mathbf{\Gamma}_m^c = 0$ for all $m < n$ and consider the evolution of the set of vectors $\mathbf{\Gamma}_n^c(t) = \mathbf{\Gamma}(t) + \delta\mathbf{\Gamma}_n^c$. It can be shown that the nth Lyapunov exponent is then given by

$$\lambda_n = \lim_{t\to\infty} \lim_{\delta\mathbf{\Gamma}_n^c \to 0} \frac{1}{\mathrm{t}} \ln\left(\frac{\left|\delta\mathbf{\Gamma}_n^c(t)\right|}{\left|\delta\mathbf{\Gamma}_n^c(0)\right|} \right) \tag{9}$$

The CPR [1, 5, 6] states that in the limit as $t \to \infty$, for every exponent λ_i there is a conjugate $\lambda_{i'}$ such that $\lambda_i + \lambda_{i'} = \chi$, where χ is constant for every i, i'. A small number of exponents, that does not grow with N, might be excluded due to their association with conserved quantities or if they correspond to displacement vectors in the direction of flow. It should also be clear that these trivial exponents for isokinetic-isobaric dynamics possess identical values to those at *NVT* and their rationale can be deduced along the same lines of Section III.C in [7].

As said, even though sufficient conditions on CPR have yet to be found [24], it has been proven that conjugate pairing occurs for a thermostatted system whose adiabatic equations of motion are Hamiltonian, as for the SLLOD PEF algorithm [5, 37], and there is clear numerical evidence that non Hamiltonian SLLOD PSF does not comply with it, although deviations are often small [6, 7].

An established and well-known link between the sum of the Lyapunov exponents and the viscosity of systems under PSF or PEF exists. Defining nonequilibrium shear viscosity as

$$\eta_{PSF} = -\frac{\langle P_{xy} \rangle}{\dot{\gamma}} \tag{10}$$

and the analogous elongation viscosity as

$$\eta_{PEF} = -\frac{\langle P_{xx} \rangle - \langle P_{yy} \rangle}{4\dot{\varepsilon}} \tag{11}$$

it can be shown [9, 14] that, neglecting terms of order $O(1/N)$, for a system under isokinetic or isoenergetic constrained dynamics we have:

$$\eta_{PSF} = -\frac{k_B \langle T \rangle}{\dot{\gamma}^2 V} \sum_{i=1}^{2dN} \lambda_i \tag{12}$$

for PSF systems and

$$\eta_{PEF} = -\frac{k_B \langle T \rangle}{4\dot{\varepsilon}^2 V} \sum_{i=1}^{2dN} \lambda_i \tag{13}$$

for PEF systems, where the brackets indicate a time average over the steady state, which is necessary in the isoenergetic case. The summation index in formulae (12)-(13) needs the slight modification $2dN \to (2dN+2)$ to accommodate for the two extra Lyapunov exponents associated with the barostatting equations (6)-(7) . We anticipate that this couple of exponents displays a conjugate pairing to zero for either equilibrium and nonequilibrium dynamics, so that Eqs. (12)-(13) are still valid for a system at *NpT* and summation can be carried out on the exponents related to the variables $(\mathbf{r}_i, \mathbf{p}_i)$ only. Also, if the system obeys CPR, the term for the sum of the exponents can be replaced with a single sum of exponents of our choosing. For example, if we use the maximum and the minimum exponents, $\sum_{i=1}^{2dN} \lambda_i \to dN(\lambda_{\max} + \lambda_{\min})$ can be substituted into Eqs (12)-(13) [5].

Lyapunov exponents can be also used to evaluate the fractal dimension of the attractor that the phase space collapses on when the system is in a steady state [2, 4, 8, 38]. This dimension can be calculated using the Kaplan-Yorke conjecture [39-41], which leads to the following formula for the embedded dimension of the attractor in the phase space:

$$D_{KY} = \frac{\sum_{i=1}^{M} \lambda_i}{|\lambda_{M+1}|} \tag{14}$$

where the exponents are ordered such that $\lambda_1 > \lambda_2 > \lambda_3 \ldots$ and M is the largest integer for which $\sum_{i=1}^{M} \lambda_i > 0$.

In the following, the aim of our study is twofold. First, a comparison is proposed between Lyapunov spectra for nonequilibrium samples at *NVT* and at *NpT*. A target pressure for the latter equal to the average pressure at constant temperature and volume is imposed, according to the data presented in [7]. These phase points belonging to different ensembles are equivalent in the extended space of thermodynamic variables given by (p, T, V, $\dot{\gamma}$) or (p, T, V, $\dot{\varepsilon}$) [42, 43] and this gives us the possibility to assess how the two different constraining procedures affect chaoticity. Then, we provide an analysis of the two exponents associated with the degrees of freedom of the NH mechanism $\left(V, \dot{\xi}\right)$, focusing on their compliance with CPR at different state points for both flows. Interestingly, results appear to be independent of the accuracy with which the pressure is conserved and unrelated to the symplecticity of the algorithms that describe the flows.

3. Details of simulations.

A 4^{th} order Gear predictor-corrector integrator [44] is employed to compute the reduced version of SLLOD equations (2) and (4), together with Eqs. (5)-(6) for pressure conservation. As said, the scheme by Benettin *et al.* is used, with a Gram-Schmidt orthogonalization method which is executed at every timestep. Notable differences from previous calculations for systems at *NVT* [1, 6-10] reside either in the smaller timestep used for *NpT*, e.g. $\Delta t = 10^{-5}$, and in the fact that our analysis is limited to spectra of two dimensional systems with 8 particles only, with density $\rho = 0.3$ and temperature $T = 1.0$. The reason for the first choice is related to a peculiar numerical instability of tangent vectors that affects systems coupled to a NH mechanism, which is independent of the integration scheme and occurs even at equilibrium or for autonomous dynamics. In fact, it turns out that numerical roundoff and finite timestep cause some $\delta\mathbf{\Gamma}_n^c(t)$ to improperly rotate into the direction of the flow, even for autonomous dynamics. This leads to a systematic error in the Lyapunov exponent associated with this particular direction, which is known to be zero for autonomous dynamics [1], and jeopardizes the orthogonality of the whole basis set of vectors [45]. If the dynamics is autonomous, this problem can be avoided by either removing components of the tangent vector lying in this direction of the flow [46], or through a significant decrease in the timestep. In our case where the dynamics is non-autonomous, a similar error is expected but, as the vector in the direction of the flow is no longer an eigenvector, we cannot simply

correct for this error and we need to reduce the timestep. As for our previous calculations at *NVT*, we prefer to sample the full *2dN+2* phase space and avoid the introduction of an explicit constraint on the vectors, to be sure that no false condition is inadvertently introduced. For the chosen Δt, we have verified that the values of the trivial exponent for $\dot{\mathbf{\Gamma}}(t)$ are correct, for each run, at equilibrium and nonequilibrium. As it will be evident shortly, a treatment of smaller size systems alone is also justified by the close analogy between *NpT* and *NVT* spectra, and by the need of calculating the exponents associated with $\left(V,\dot{\xi}\right)$ for a number of different state points. This task appears to be computationally demanding for larger atomic samples at an equivalent Δt.

In the same fashion of [7], the phase space contraction factor $\Lambda\left(\mathbf{\Gamma}\right)=\partial/\partial\mathbf{\Gamma}\cdot\mathbf{\Gamma}$ for a two dimensional PSF system is given by

$$\left\langle \Lambda_{PSF}^{NpT}\right\rangle=\sum_{i=1}^{4N+2}\lambda_i=\left\langle -\alpha(2N-1)+\dot{\gamma}\frac{\sum_{i=1}^{N}p_{xi}\ p_{yi}}{\sum_{i=1}^{N}\mathbf{p}_i\cdot\mathbf{p}_i}+2\dot{\xi}\right\rangle \tag{15}$$

and by

$$\left\langle \Lambda_{PEF}^{NpT}\right\rangle=\sum_{i=1}^{4N+2}\lambda_i=\left\langle -\alpha(2N-1)+\dot{\varepsilon}\frac{\sum_{i=1}^{N}(p_{xi}^2-p_{yi}^2)}{\sum_{i=1}^{N}\mathbf{p}_i\cdot\mathbf{p}_i}+2\dot{\xi}\right\rangle \tag{16}$$

for PEF, where brackets denote a time average and the first sums are extended to the two NH degrees of freedom. These expressions differ from their isokinetic

counterparts for the contribution of the piston-like term $\langle \dot{\xi} \rangle$, which, according to the evolution equation for the volume (6), is expected to decrease to zero in the long time limit*, i.e. $\langle \dot{\xi} \rangle \to 0$. In fact, once the system has reached a steady state, the average volume and pressure undergo smaller and smaller oscillations around their constant target values and the dynamics becomes equivalent to that of a isokinetic-isochoric ensemble. This means that comparable $\langle \Lambda(\mathbf{\Gamma}) \rangle$ have to be found at *NpT* and *NVT* when values of Gaussian thermostats are similar, as we will show in the following. Furthermore, the difference between the sum of all Lyapunov exponents and the ensemble average in the right hand side of Eqs. (15)-(16) will be referred to as the deviation. In Table 1 we indicate the maximum value of the deviation at the end of the runs as a percentage of the computed $\sum_{i=1}^{2dN+2} \lambda_i$ for every state point: the disagreement is less than 0.04% of the value of the sum at each check and the maximum difference does not change considerably after t = 100. This also means that, as the runs start from a face-centered cubic lattice, the equilibration of the systems is not influencing the final values of the exponents. As an indication, the initial transient period (when the convergence of the exponents is still not optimal) ends approximately at $t \sim 1.0$. We have also reported in Table 1 relevant quantities for Lyapunov spectra, nonequilibrium viscosity and the Kaplan-Yorke dimension for the isokinetic-isobaric samples. In general, all the results have been collected

* For our systems, numerical data also show that $\langle \dot{\xi} \rangle$ is very small and negligible with respect to the other terms in Eqs. (15)-(16) approximately after $t \sim 1$.

from three independent runs with random initial peculiar momenta and for a total simulation time t = 10000. This, and a chosen damping factor $Q = 10^6$, assure that the requirements discussed in [30] regarding the character of pressure fluctuations are correctly met.

4. Results for Lyapunov spectra and conjugate pairing for Nosé-Hoover degrees of freedom.

Let us start our discussion by inspecting Table 1 and comparing it with analogous data in Table 1 of [7] for *NVT* systems. Results for viscosities from direct NEMD calculations (Eqs. (10)-(11)), from expressions involving the sum of the exponents (Eqs. (12)-(13)) and from application of CPR with ($\lambda_{\max}$ + $\lambda_{\min}$) are also reported. Firstly, simulations at *NpT* display a smaller value for the isokinetic multiplier than their counterparts at constant volume. This can be understood by considering that the average V for equilibrium and nonequilibrium collections of atoms at *NpT* is always larger than the *NVT* case. On average, the action of the NH mechanism causes the distances among the particles to increase, with a consequent decrease in $\mathbf{F}_i$. Thus, according to the equations of motion, the rate of change for the momenta $\dot{\mathbf{p}}_i$ is then affected, and this is responsible for reducing the amount of heat that has to be extracted by the thermostat at *NpT*. We can equivalently affirm that, to

maintain the target pressure, the system expands at the expense of its own internal energy, reducing the work required by the thermostat to achieve the same temperature as in *NVT*.

Differences in α lead to unequal phase space compression factors and allow for a further check on the validity of our calculations. In fact, besides the excellent results for the deviation reported in Table 1 which show very accurate cumulative sums for all the exponents, one can subtract $\left\langle \Lambda^{NVT} \right\rangle$ from $\left\langle \Lambda^{NpT} \right\rangle$ for equivalent state points and, assuming that $\left\langle \dot{\xi} \right\rangle = 0$ and neglecting terms of 1 in N, obtain the following expression

$$\left\langle \Lambda^{NpT} \right\rangle - \left\langle \Lambda^{NVT} \right\rangle = -(2N-1)\left[\left\langle \alpha^{NpT} \right\rangle - \left\langle \alpha^{NVT} \right\rangle \right] \tag{17}$$

where the superscripts indicate the type of ensemble. Using data from the simulations discussed in [7], the agreement between the two sides of the above formula is satisfactory and confirms the reliability of our evaluations (see Table 2).

Considering Table 1, some more features are worth addressing. As expected, viscosities calculated with NEMD time averages do not change across the two thermodynamic regimes, and the values obtained using the sum of Lyapunov exponents and expressions (12)-(13) are very close also for *NpT*. This stresses the equivalence between state points in the extended space of thermodynamic observables, as previously discussed. Secondly, the differences between Kaplan-Yorke dimensions of the attractors between *NpT* and *NVT* ensembles is always two, due to the presence of the couple of degrees of freedom $\left(V, \dot{\xi}\right)$ in the former. This

fact shows that the dimensional collapse occurs only in the ordinary variables $(\mathbf{r}_i, \mathbf{p}_i)$ and does not involve the NH coordinates, which neither undergo contraction, nor contribute any increase in the overall shrinkage in the phase space. An intuitive reason is given once more by the differences in final volumes between the simulation cells in the two ensembles: on average, the NH barostat does not exert work on the system and does not enhance or suppress its disorder or its dissipation. This, according to the entropy rate formula $\dot{S} = -k_B \sum_{i=1}^{2dN} \lambda_i$ for isokinetic *NVT* systems from which Eqs. (12)-(13) are derived, is the ultimate cause for the existence of a low dimensional attractor [9, 14]. The fact that the two extra NH exponents sum to zero, as we will show shortly, is clearly in agreement with the observation above and the substitution $2dN \rightarrow (2dN + 2)$ has no effect on the value of $\dot{S}$.

If Lyapunov spectra are closely considered, discrepancies arise between the thermodynamical constraints of interest, as it can also be deducted from a comparison of the values of $\lambda_{\max}$ and $\lambda_{\min}$ with their *NVT* analogues. Further insight can be gained by analyzing the differences $\Delta\lambda_i$ between exponents with the same numbers in *NpT* and *NVT* steady states, as pictured in Figs. 1-3. Results for equilibrium and nonequilibrium samples are at increasing, equivalent II, i.e. the second scalar invariant of the strain rate tensor. This quantity is defined as $2\dot{\gamma}^2$ for PSF and $8\dot{\varepsilon}^2$ for PEF, and its value represents a measure of energy dissipation in a viscous fluid [47].

It is evident from Fig. 4.11 that the presence of the NH barostat induces a small and roughly sinusoidal symmetric shift in the values of the exponents with respect to an equilibrium simulation at constant volume. This effect is related to the increased dimension of tangent vectors $\delta\mathbf{\Gamma}_n^c(t)$, which span a larger tangent space that comprises the directions associated with V and $\dot{\xi}$. Displacements along these coordinates affect the Lyapunov instability of all the degrees of freedom in the system, as every vector in the basis set contains non vanishing infinitesimal increments δV and $\delta\dot{\xi}$. Nonetheless, because of its symmetrical character, the appearance of this shift in *NpT* samples does not alter the previous results about the compliance to CPR which have been thoroughly discussed in [7], as these contributions are independent of the type of flow considered (see Figs. 2-3). In fact, at equilibrium, exponents belonging to the same conjugate pair are displaced by opposite and equal contributions, so that CPR still occurs for every sum at zero. At nonequilibrium, the difference ΔCPR in the values of χ among sums at *NVT* and *NpT* is mainly due to unequal values of the respective isokinetic multipliers α, and has to be accounted for. This disparity depends also on II, as Table 2 indicates, and its value identifies the symmetric axis around which the *NpT-NVT* differences between exponents $\Delta\lambda_i$ are distributed. According to Figs. 2-3, shifts relative to ΔCPR do not appear to sensitively change with the increase in flow rates and generally conserve the same shape they display at equilibrium.

The only exception is given by PSF at $\dot{\gamma} = 2.0,$ which presents a jump in the centre of the differences profile, as plotted in Fig. 3. This can be dependent on how the two distinct flows, PEF and PSF, affect the slowest growing (or decaying) phenomena in the sample. As explained in [48, 49], values of the smallest positive (and negative) exponents in the middle of the Lyapunov spectrum are closely related to the collective, highly delocalized events in the system. In Figs. 1-3, the magnitude of $\Delta\lambda_i$ seems to be generally lower for the smallest exponents, indicating that the slowest events among the particles are the least affected by the instability coming from the NH variables V and $\dot{\xi}$. If we now inspect our previous results in Figs. 2 and 6[†] in [7] for constant volume, which show the differences for exponents at nonequilibrium and equilibrium for different flows, we can notice that PSF has the tendency to increase the gap among those small λ_i that lie in the centre of the spectrum, whereas PEF is characterized by an almost homogeneous shift for all the atomic degrees of freedom. All this means is that, with respect to equilibrium, planar shear appears to increase the velocity of those (slow) events that

igher the exponent and ultimately the bigger the jump $\Delta\lambda_i$ due to the presence of the NH barostat, the heterogeneous behaviour of the shifts in Fig. 3 seems to arise from flow-dependent perturbations in the time scales for the collective events in the

[†] It has to be noted that the data in these figures are not plotted with respect to the conjugate pairing constant χ. The effective contribution to the middle of the spectrum due to $\dot{\gamma}$ should be evaluated across this χ – line instead. Note that the profiles are qualitatively similar to Figs. 1-3 in this work.

The second part of our analysis is devoted to the investigation of compliance to CPR for the two exponents belonging to the extra coordinates $\left(V,\dot{\xi}\right)$ peculiar to the *NpT* ensemble. Their values λ_+ and λ_- have been collated in Table 3, for various PSF and PEF state points. For equilibrium, planar elongation and planar shear up to a moderate rate $\dot{\gamma}=1.0,$ it is found that $\lambda_+ + \lambda_- = 0$ regardless of the density, pressure and temperature of the sample. Not only do the sums conserve, but the magnitudes of the exponents can be considered invariant with respect to the state point, and the type and strength of the applied field, being $\lambda_\pm \approx \pm 0.021$. Interestingly, even when the target pressure cannot be maintained by the integral feedback mechanism with a high accuracy, CPR at zero still holds for the NH couple, as it can be seen from the simulations labeled as B for $\dot{\gamma}=1.0$ in Table 3. Given the very small system size, the precision displayed by the barostat strongly depends on the chosen target pressure and the selected value for the temperature. In some sense, the Gaussian and NH mechanisms are simultaneously competing for the available kinetic energy K so that T and p (see Eqs. (3), (5) and (8)) can attain the input values set by the user. According to the values of ρ, p_0 and T_0, an 8 particle system may not possess sufficient internal energy to undergo the volume expansion required to reach p_0, because a substantial part of K has been already constrained by α, which acts instantaneously to preserve the chosen temperature T_0. This is clearly seen by comparing quantities in simulations B and C in Table 3, noticing how the robust increase in p_0 for the latter corresponds to a sensitive

improvement in the conservation of the pressure with respect to runs B. Generally, for identical values of ρ, T_0 and $\dot{\gamma}$, a higher target pressure is achieved at a smaller target volume, with a consequently lower amount of work done by the system.

A justification of the zero value for the sum between λ_+ and λ_- can be provided by looking at Eqs. (15) and (16). For equilibrium, the second term at the right hand side vanishes for both expressions, and, as said, $\left\langle \Lambda_{EQ}^{NpT} \right\rangle$ differs from $\left\langle \Lambda_{EQ}^{NVT} \right\rangle$ only for the contribution proportional to $\left\langle \dot{\xi} \right\rangle$. As this contribution goes to zero at large times, and since the CPR is still valid with $\chi = 0$, the net effect of the NH degrees $\left(V, \dot{\xi}\right)$ in the phase space contraction has to be null, and the pair assumes values such that $\lambda_+ + \lambda_- = 0$. For PSF and PEF, it can be seen in Eqs. (6) and (7) that no terms related to nonequilibrium explicitly enter the NH dynamics. As detailed in the Appendix, the elements of the stability matrix **T**, and consequently the equation for the vectors $\delta\dot{\mathbf{\Gamma}}(t) = \mathbf{T}(t) \cdot \delta\mathbf{\Gamma}(t)$, have the same expressions at equilibrium and nonequilibrium for the vector components associated with $\left(V, \dot{\xi}\right)$. Loosely speaking, this couple of coordinates is blind to the underlying evolution of $\left(\mathbf{r}_i, \mathbf{p}_i\right)$ and has no knowledge that the atoms are out of equilibrium. Those equations only serve the purpose of providing the target V and the magnitude of the piston-like term $\dot{\xi}$ to conserve the desired p_0. This, together with the formulae for $\left\langle \Lambda_{PSF}^{NpT} \right\rangle$ and $\left\langle \Lambda_{PEF}^{NpT} \right\rangle$, explain why the sum $\left(\lambda_+ + \lambda_-\right)$ is preserved at equilibrium and neither value of the exponents changes. As said, an indirect

confirmation is also given by the fact that the viscosity has a common value for *NVT* and *NpT* equivalent state points (see Table 1 in [7] and Table 1 in the present work). According to Eqs. (12) and (13) and to the symmetric nature of the shift $\Delta\lambda_i$ described in Figs. 1-3, the sum $\sum_{i=1}^{4N}\lambda_i$ of the exponents pertaining to $(\mathbf{r}_i,\mathbf{p}_i)$ remains constant between the two ensembles and forces λ_+ and λ_- to sum to zero.

All the above considerations do not seem to apply to PSF at a higher rate $\dot{\gamma}=2.0,$ for which λ_+ and λ_- differ from all the previous cases and do not show a trend that can be easily related to the thermodynamic observables in the system. This fact might be connected to the appearance of strings in analogous *NVT* runs [50] and to the poor compliance with CPR observed in [6, 7]. Simulations labeled as D in Table 3 do show a zero conjugate pairing for λ_+ and λ_- at a temperature and density where lanes are less likely to occur than for labels A, B and C [51], but the values of the exponents are different from those found for the equivalent phase point at PEF, which remains identical to equilibrium. For this reason, we can only state that, at this particular value of the flow rate, the sum of the exponents associated with the barostatting procedure is sensitive to the state point.

5. Conclusions

In conclusion, we have proved that CPR for *NpT* spectra generally maintains the same accuracy observed in the case of *NVT* simulations, and that the presence of a

NH barostat gives rise to the appearance of two conjugate exponents, whose values are independent of the thermodynamical quantities of the systems and whose sum is always equal to zero, for equilibrium and nonequilibrium samples. Apart from the case of PSF at $\dot{\gamma} = 2.0$, which requires further investigation, the two thermodynamic ensembles present closely similar chaotic properties, and the simultaneous use of a NH mechanism for constant pressure and a Gaussian thermostat does not alter the dimension of the attractor in the $(\mathbf{r}_i, \mathbf{p}_i)-$space with respect to analogous isokinetic-isochoric ensembles. Compared to these, an integral feedback mechanism homogeneously rearranges the Lyapunov exponents in such a way that no modification of the overall chaoticity of the system takes place. This is intuitively expected because the NH equations of motion that constrain the pressure are insensitive to the nonequilibrium contributions present in the underlying atomic dynamics, and because *NpT* and *NVT* phase space trajectories at the "extended" state point (N, p, T, V) are actually identical, giving rise to equal dissipation-related contractions which in turn force the "extra" NH couple of exponents to sum to zero.

Acknowledgements

We thank the Australian Government for financial assistance.

Appendix. Expressions for the elements of the stability matrix for the isokinetic-isobaric ensemble.

We explicitly derive the coefficients of the stability, or Jacobian, matrix $\mathbf{T}$ defined as $\partial\dot{\mathbf{\Gamma}}/\partial\mathbf{\Gamma}$, where $\dot{\mathbf{\Gamma}}=\mathbf{G}\left(\mathbf{\Gamma},t\right)$ are the equations of motion given for equilibrium and nonequilibrium systems in the *NpT* ensemble. The presence of Eqs. (6) and (7) for the NH barostat causes the dimension of the phase space to be $dN+2$, where *d* is the Cartesian dimension, *N* is the number of atoms and 2 are the extra degrees of freedom $\left(V,\dot{\xi}\right)$. In general, the stability matrix is thus expressed as

$$\mathbf{T}^{NpT}=\begin{pmatrix} \frac{\partial\dot{\mathbf{r}}}{\partial\mathbf{r}} & \frac{\partial\dot{\mathbf{r}}}{\partial\mathbf{p}} & \frac{\partial\dot{\mathbf{r}}}{\partial V} & \frac{\partial\dot{\mathbf{r}}}{\partial\dot{\xi}} \\ \frac{\partial\dot{\mathbf{p}}}{\partial\mathbf{r}} & \frac{\partial\dot{\mathbf{p}}}{\partial\mathbf{p}} & \frac{\partial\dot{\mathbf{p}}}{\partial V} & \frac{\partial\dot{\mathbf{p}}}{\partial\dot{\xi}} \\ \frac{\partial\dot{V}}{\partial\mathbf{r}} & \frac{\partial\dot{V}}{\partial\mathbf{p}} & \frac{\partial\dot{V}}{\partial V} & \frac{\partial\dot{V}}{\partial\dot{\xi}} \\ \frac{\partial\ddot{\xi}}{\partial\mathbf{r}} & \frac{\partial\ddot{\xi}}{\partial\mathbf{p}} & \frac{\partial\ddot{\xi}}{\partial V} & \frac{\partial\ddot{\xi}}{\partial\dot{\xi}} \end{pmatrix} \tag{A1}$$

where the reduced coordinate is defined as $\mathbf{r}_i=\mathbf{q}_i/V^{1/d}$, $\mathbf{q}_i$ are laboratory positions and $\mathbf{p}_i$ are the peculiar momenta, as described above. If we indicate the Cartesian components with Greek letters $\alpha,\beta,...$ and the particle numbers with indices $i,j,...$, derivations of Eqs. (2) and (4) for PSF and PEF provide the following terms for $\dot{r}_{\beta j}$:

$$
\begin{aligned}
&\frac{\partial}{\partial r_{\alpha i}}\dot{r}_{\beta j} = \begin{cases} \dot{\gamma}\delta_{\alpha y}\delta_{\beta x}\delta_{ij} & \text{for shear} \\ \left(\dot{\varepsilon}\delta_{\alpha x}\delta_{\beta x} - \dot{\varepsilon}\delta_{\alpha y}\delta_{\beta y}\right)\delta_{ij} & \text{for elongation} \end{cases} \\
&\frac{\partial}{\partial p_{\alpha i}}\dot{r}_{\beta j} = \frac{\delta_{\alpha\beta}\delta_{ij}}{mV^{1/d}} \\
&\frac{\partial}{\partial V}\dot{r}_{\beta j} = -\frac{p_{\beta j}}{dmV^{(1/d+1)}} \\
&\frac{\partial}{\partial \dot{\xi}}\dot{r}_{\beta j} = 0
\end{aligned}
\tag{A2}
$$

and analogously for $\dot{p}_{\beta j}$:

$$
\begin{aligned}
&\frac{\partial}{\partial r_{\alpha i}}\dot{p}_{\beta j} = \frac{\partial F_{\beta j}}{\partial r_{\alpha i}} - \frac{\partial \alpha}{\partial r_{\alpha i}}p_{\beta j} \\
&\frac{\partial}{\partial p_{\alpha i}}\dot{p}_{\beta j} = -\alpha\delta_{\alpha\beta}\delta_{ij} - \frac{\partial \alpha}{\partial p_{\alpha i}}p_{\beta j} + \begin{cases} -\dot{\gamma}\delta_{\alpha y}\delta_{\beta x}\delta_{ij} & \text{for shear} \\ -\left(\dot{\varepsilon}\delta_{\alpha x}\delta_{\beta x} - \dot{\varepsilon}\delta_{\alpha y}\delta_{\beta y}\right)\delta_{ij} & \text{for elongation} \end{cases} \\
&\frac{\partial}{\partial V}\dot{p}_{\beta j} = \frac{\partial F_{\beta j}}{\partial V} - \frac{\partial \alpha}{\partial V}p_{\beta j} \\
&\frac{\partial}{\partial \dot{\xi}}\dot{p}_{\beta j} = 0
\end{aligned}
\tag{A3}
$$

where $F_{\beta j}$ is the force on component β experienced by particle *j*, and α is the Gaussian thermostat multiplier (see Eq. (3) for PSF and (5) for PEF). Before the expressions for the derivatives in (A3) are provided, let us report the elements associated with Eqs. (6) and (7):

$$
\begin{aligned}
&\frac{\partial}{\partial r_{\alpha i}}\dot{V} = 0 \\
&\frac{\partial}{\partial p_{\alpha i}}\dot{V} = 0 \\
&\frac{\partial}{\partial V}\dot{V} = d\dot{\xi} \\
&\frac{\partial}{\partial \dot{\xi}}\dot{V} = dV
\end{aligned}
\tag{A4}
$$

and

$$\begin{aligned}
&\frac{\partial}{\partial r_{\alpha i}}\ddot{\xi} = \frac{\partial p}{\partial r_{\alpha i}}\frac{V}{NQk_BT} \\
&\frac{\partial}{\partial p_{\alpha i}}\ddot{\xi} = \frac{2Vp_{\alpha i}}{dNQk_BT} \\
&\frac{\partial}{\partial V}\ddot{\xi} = \frac{\left(p-p_0\right)}{NQk_BT} + \frac{\partial p}{\partial V}\frac{V}{NQk_BT} \\
&\frac{\partial}{\partial \dot{\xi}}\ddot{\xi} = 0
\end{aligned} \tag{A5}$$

where p is the trace of the pressure tensor (8) divided by the dimensionality d, Q is the damping factor and p_0 is the target pressure. As it can be seen, formulae (A3) and (A5) contain derivatives of the force $\mathbf{F}_i$, which needs to be expressed in terms of the reduced coordinates $\mathbf{r}_i = \mathbf{q}_i / V^{1/d}$. We can introduce the constants a and b, defined as

$$\begin{aligned}
a &= V^{-7/d} \\
b &= V^{-6/d} = aV
\end{aligned}$$

and obtain the expression for the force in terms of $r = \left\|\mathbf{r}_i - \mathbf{r}_j\right\| = \left\|\mathbf{q}_i - \mathbf{q}_j\right\| / V^{1/d}$:

$$\mathbf{F}_{ij}(\mathbf{r}_i, \mathbf{r}_j) = \frac{24a}{r^8}\left(\frac{2b}{r^6} - 1\right)\left[\mathbf{r}_i - \mathbf{r}_j\right] \tag{A6}$$

It is clear that the value of (A6) is identical to the one that comes from the usual derivation of the potential (1) with respect to ordinary laboratory distances. Nonetheless, $\mathbf{F}_{ij}(\mathbf{r}_i, \mathbf{r}_j)$ is now a function of $\mathbf{r}_i$ and of the volume V, and it needs to be used when calculating the terms $\frac{\partial \alpha}{\partial r_{\alpha i}}$, $\frac{\partial p}{\partial r_{\alpha i}}$ and $\frac{\partial p}{\partial V}$. Given the definition (8), the

last derivative gives the contribution $\frac{\partial \mathbf{F}_{ij}(\mathbf{r}_i,\mathbf{r}_j)}{\partial V}$, which, for a component α, can be written as

$$\frac{\partial F_{\alpha ij}(\mathbf{r}_i,\mathbf{r}_j)}{\partial V} = -\frac{24a}{dVr^8}\left(\frac{26b}{r^6}-7\right)\left[r_{\alpha i}-r_{\alpha j}\right] \tag{A7}$$

Expressions for $\frac{\partial F_{\alpha ij}(\mathbf{r}_i,\mathbf{r}_j)}{\partial r_{\beta j}}$ are analogous to those found for the usual $\frac{\partial F_{\alpha ij}(\mathbf{q}_i,\mathbf{q}_j)}{\partial q_{\beta j}}$ and are omitted here. The derivatives of the isokinetic multiplier are identical to the ones found for an *NVT* ensemble, except for the substitution $\frac{\partial F_{\alpha ij}(\mathbf{q}_i,\mathbf{q}_j)}{\partial q_{\beta j}} \rightarrow \frac{\partial F_{\alpha ij}(\mathbf{r}_i,\mathbf{r}_j)}{\partial r_{\beta j}}$,

$$\begin{aligned}
&\frac{\partial}{\partial r_{\beta j}}\alpha = \frac{\sum_{\alpha i}\partial F_{\alpha i}/\partial r_{\beta j}\cdot p_{\alpha i}}{\sum_{\alpha i}p_{\alpha i}^2}\\
&\frac{\partial}{\partial p_{\beta j}}\alpha = \begin{cases}\dfrac{F_{\beta j}-2\alpha p_{\beta j}-\dot\gamma\left(\delta_{\beta x}p_{yj}+\delta_{\beta y}p_{xj}\right)}{\sum_{\alpha i}p_{\alpha i}^2} & \text{for shear}\\ \dfrac{F_{\beta j}-2\alpha p_{\beta j}-2\dot\varepsilon\left(\delta_{\beta x}-\delta_{\beta y}\right)p_{\beta j}}{\sum_{\alpha i}p_{\alpha i}^2} & \text{for elongation}\end{cases}\\
&\frac{\partial}{\partial V}\alpha = \frac{\sum_{\alpha i}\partial F_{\alpha i}/\partial V\cdot p_{\alpha i}}{\sum_{\alpha i}p_{\alpha i}^2}
\end{aligned} \tag{A8}$$

whereas the derivative of *p* respect to the component $r_{\alpha i}$ are given by

$$\frac{\partial}{\partial r_{\alpha i}}p = \frac{1}{dV^{(1-1/d)}}\left[\sum_j F_{\alpha ij}+\sum_{\beta j}\frac{\partial F_{\beta ij}}{\partial r_{\alpha i}}\left(r_{\beta i}-r_{\beta j}\right)\right] \tag{A9}$$

It is possible to write the evolution equation for the tangent vectors in a compact form, which, for equilibrium, turns out to be

$$
\begin{aligned}
\delta\dot{\mathbf{r}} &= \frac{\partial\dot{\mathbf{r}}}{\partial\mathbf{p}}\cdot\delta\mathbf{p} + \frac{\partial\dot{\mathbf{r}}}{\partial V}\delta V \\
\delta\dot{\mathbf{p}} &= \frac{\partial\dot{\mathbf{p}}}{\partial\mathbf{r}}\cdot\delta\mathbf{r} + \frac{\partial\dot{\mathbf{p}}}{\partial\mathbf{p}}\cdot\delta\mathbf{p} + \frac{\partial\dot{\mathbf{p}}}{\partial V}\delta V \\
\delta\dot{V} &= \frac{\partial\dot{V}}{\partial V}\delta V + \frac{\partial\dot{V}}{\partial\dot{\xi}}\delta V \\
\delta\dot{\xi} &= \frac{\partial\ddot{\xi}}{\partial\mathbf{r}}\cdot\delta\mathbf{r} + \frac{\partial\ddot{\xi}}{\partial\mathbf{p}}\cdot\delta\mathbf{p} + \frac{\partial\ddot{\xi}}{\partial V}\delta V
\end{aligned}
\tag{A10}
$$

The dynamics of the infinitesimal displacements $\delta\mathbf{\Gamma} = \left[\delta\mathbf{r},\ \delta\mathbf{p},\ \delta V,\ \delta\dot{\xi}\right]$ can be explicitly determined by substituting the previous formulae (A2)-(A9) in the above equations. When a nonequilibrium PSF or PEF system is considered, the SLLOD terms associated with shear and elongational fields cause the emergence of the extra factor $\frac{\partial\dot{\mathbf{r}}}{\partial\mathbf{r}}\cdot\delta\mathbf{r}$ in the equation for $\delta\dot{\mathbf{r}}$ which is detailed in (A2), and modify the form of $\frac{\partial\dot{\mathbf{p}}}{\partial\mathbf{p}}\cdot\delta\mathbf{p}$ as pointed out in (A3). Further, derivatives of the thermostat multipliers with respect to $r_{\beta j}$ and $p_{\beta j}$ do depend on the type of flow. Nonetheless, it is important to note that these discrepancies between equilibrium and nonequilibrium affect *only* the components $\delta\mathbf{r}$ and $\delta\mathbf{p}$ of the tangent vectors and solely appear in the first two lines of (A10). The remaining elements of $\mathbf{T}$ at PSF or PEF conserve the same expressions they have at equilibrium: this is ultimately the cause for the invariant and zero conjugate pairing of the Lyapunov exponents pertaining to the degrees of freedom of the NH barostat, as discussed above.

References

[1] S. S. Sarman, D. J. Evans, and G. P. Morriss, Phys. Rev. A **45**, 2233 (1992).

[2] G. P. Morriss, Phys. Lett. A **134**, 307 (1989).

[3] G. P. Morriss, Phys. Rev. E **65**, 017201 (2001).

[4] G. P. Morriss, Phys. Rev. A **37**, 2118 (1988).

[5] D. J. Evans, E. G. D. Cohen, and G. P. Morriss, Phys. Rev. A **42**, 5990 (1990).

[6] D. J. Searles, D. J. Evans, and D. J. Isbister, Chaos **8**, 337 (1998).

[7] F. Frascoli, D. J. Searles, and B. D. Todd, Phys. Rev. E **73**, 046206 (2006).

[8] H. A. Posch and W. G. Hoover, Phys. Rev. A **39**, 2175 (1989).

[9] H. A. Posch and W. G. Hoover, Phys. Rev. A **38**, 473 (1988).

[10] W. G. Hoover, H. A. Posch, and S. Bestiale, J. Chem. Phys. **87**, 6665 (1987).

[11] C. Dellago, H. A. Posch, and W. G. Hoover, Phys. Rev. E **53**, 1485 (1996).

[12] D. J. Evans and G. P. Morriss, *Statistical mechanics of nonequilibrium liquids* (Academic, New York, 1990).

[13] S. S. Sarman, D. J. Evans, and P. T. Cummings, Phys. Rep. **605**, 1 (1998).

[14] E. G. D. Cohen, Physica A **213**, 293 (1994).

[15] J. D. Weeks, D. Chandler, and H. C. Andersen, J. Chem. Phys. **54**, 5237 (1985).

[16] W. G. Hoover, Phys. Rev. A **31**, 1695 (1985).

[17] B. D. Todd and P. J. Daivis, Phys. Rev. Lett. **81**, 1118 (1998).

[18] B. D. Todd and P. J. Daivis, Comput. Phys. Commun. **117**, 191 (1999).

[19] B. D. Todd and P. J. Daivis, Mol. Sim. **33**, 189 (2007).

[20] A. Baranyai and P. T. Cummings, J. Chem. Phys. **110**, 42 (1999).

[21] V. I. Arnold and A. Avez, *Ergodic Problems of Classical Mechanics* (Addison-Wesley, New York, 1968).

[22] T. A. Hunt and B. D. Todd, Mol. Phys. **101**, 3445 (2003).

[23] A. M. Kraynik and D. A. Reinelt, Int. J. Mult. Flow **18**, 1045 (1992).

[24] R. Abraham and J. E. Marsden, *Foundations of mechanics* (Addison-Wesley, Redwood City, CA, 1987).

[25] A. J. Dragt, *Lectures on nonlinear orbit dynamics* (American Institute of Physics, AIP Conf. Proc. **87**, Woodbury, 1978).
[26] D. Panja and R. van Zon, Phys. Rev. E **66**, 021101 (2002).
[27] D. Panja and R. van Zon, Phys. Rev. E **65**, 060102 (2002).
[28] C. Braga and K. P. Travis, J. Chem. Phys. **124**, 104102 (2006).
[29] J. T. Bosko, B. D. Todd, and R. J. Sadus, J. Chem. Phys. **123**, 034905 (2005).
[30] F. Frascoli and B. D. Todd, J. Chem. Phys. **126**, 044506 (2007).
[31] A. W. Lees and S. F. Edwards, J. Phys. C: Solid State Phys. **5**, 1921 (1972).
[32] B. D. Todd and P. J. Daivis, J. Chem. Phys. **112**, 40 (2000).
[33] G. Benettin, L. Galgani, and J.-M. Strelcyn, Phys. Rev. A **14**, 2338 (1976).
[34] G. Benettin, L. Galgani, A. Giorgilli, et al., Meccanica **15**, 9 (1980).
[35] G. Benettin, L. Galgani, A. Giorgilli, et al., Meccanica **15**, 21 (1980).
[36] I. Shimada and T. Nagashima, Prog. Theor. Phys. **61**, 1605 (1979).
[37] C. P. Dettmann and G. P. Morriss, Phys. Rev. E **53**, 5545 (1996).
[38] B. L. Holian, C. G. Hoover, and H. A. Posch, Phys. Rev. Lett. **59**, 10 (1987).
[39] D. J. Evans, E. G. D. Cohen, D. J. Searles, et al., J. Stat. Phys. **101**, 17 (2000).
[40] P. Frederickson, J. L. Kaplan, and E. D. Yorke, J. Diff. Eqs. **49**, 185 (1983).
[41] L. S. Young, Ergod. Th. and Dynam. Sys. **2**, 109 (1982).
[42] D. J. Evans and A. Baranyai, Phys. Rev. Lett. **67**, 2597 (1991).
[43] P. J. Daivis and D. J. Evans, J. Chem. Phys. **100**, 541 (1994).
[44] C. W. Gear, *Numerical Initial Value Problems in Ordinary Differential Equations* (Prentice-Hall, Englewood Cliffs, NJ, 1971).
[45] S. R. Williams, *private communication*, (2007).
[46] S. R. Williams, D. J. Searles, and D. J. Evans, J. Chem. Phys. **124**, 194102 (2006).
[47] R. B. Bird, C. F. Curtiss, R. C. Armstrong, et al., *Dynamics of Polymeric Liquids* (Wiley, Volumes I and II, New York, 1987).
[48] J.-P. Eckmann, C. Forster, H. A. Posch, et al., J. Stat. Phys. **118**, 795 (2005).

[49] H. A. Posch and W. G. Hoover, Journal of Physics: Conference Series **31**, 9 (2006).

[50] D. J. Evans and G. P. Morriss, Phys. Rev. Lett. **56**, 2172 (1986).

[51] J. Delhommelle, Phys. Rev. E **71**, 016705 (2005).

Figure Captions.

Fig. 1. Differences between Lyapunov exponents at equilibrium under *NpT* and *NVT* dynamics. Trivial exponents and the couple due to the degrees of freedom $\left(V, \dot{\xi}\right)$ are omitted, and are not considered also in Figs. 2-3.

Fig. 2. Differences between Lyapunov exponents for moderate shear and elongational rates, under *NpT* and *NVT* dynamics. The dotted and dashed lines respectively represent the averages of $\Delta\lambda_i$ for PEF and PSF. These lines also correspond to half the shift in the conjugate pairing constant between the two regimes, as indicated in Table 2.

Fig. 3. Differences between Lyapunov exponents for high shear and elongational rates, under *NpT* and *NVT* dynamics. The dotted and dashed lines have the same meaning as in Fig. 2.

Fig. 1. Frascoli *et al*

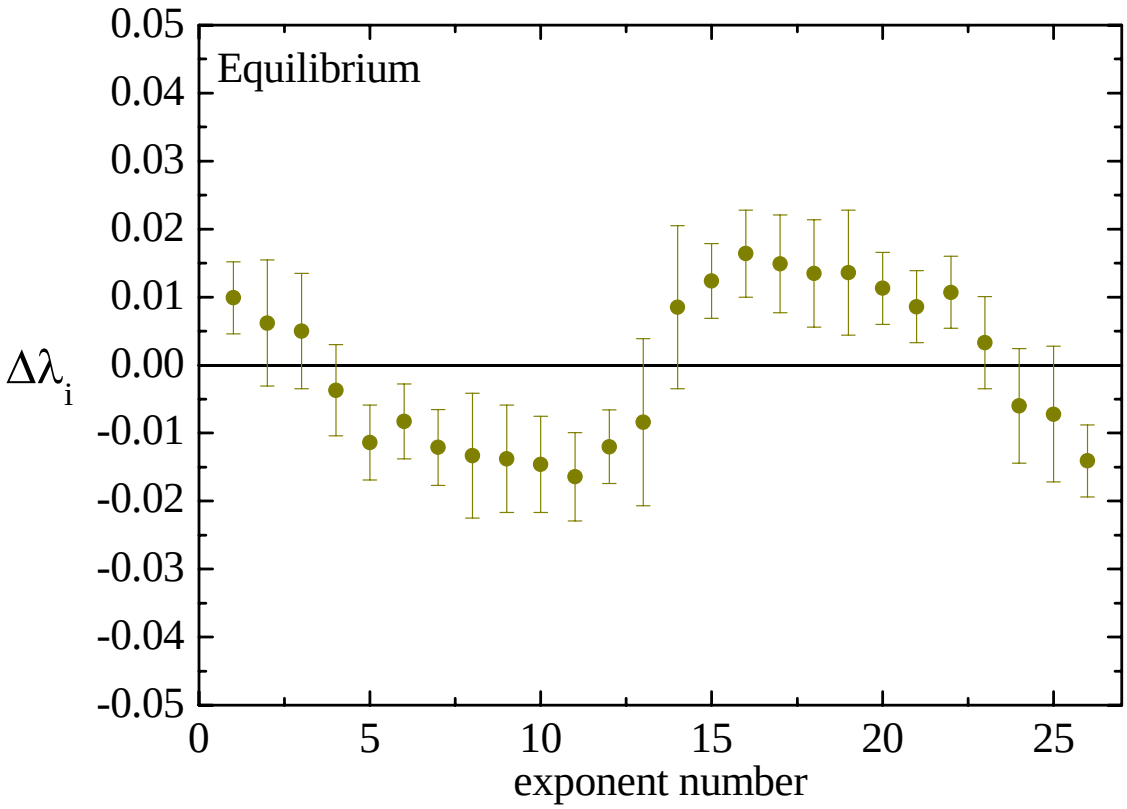

Fig. 2. Frascoli *et al*

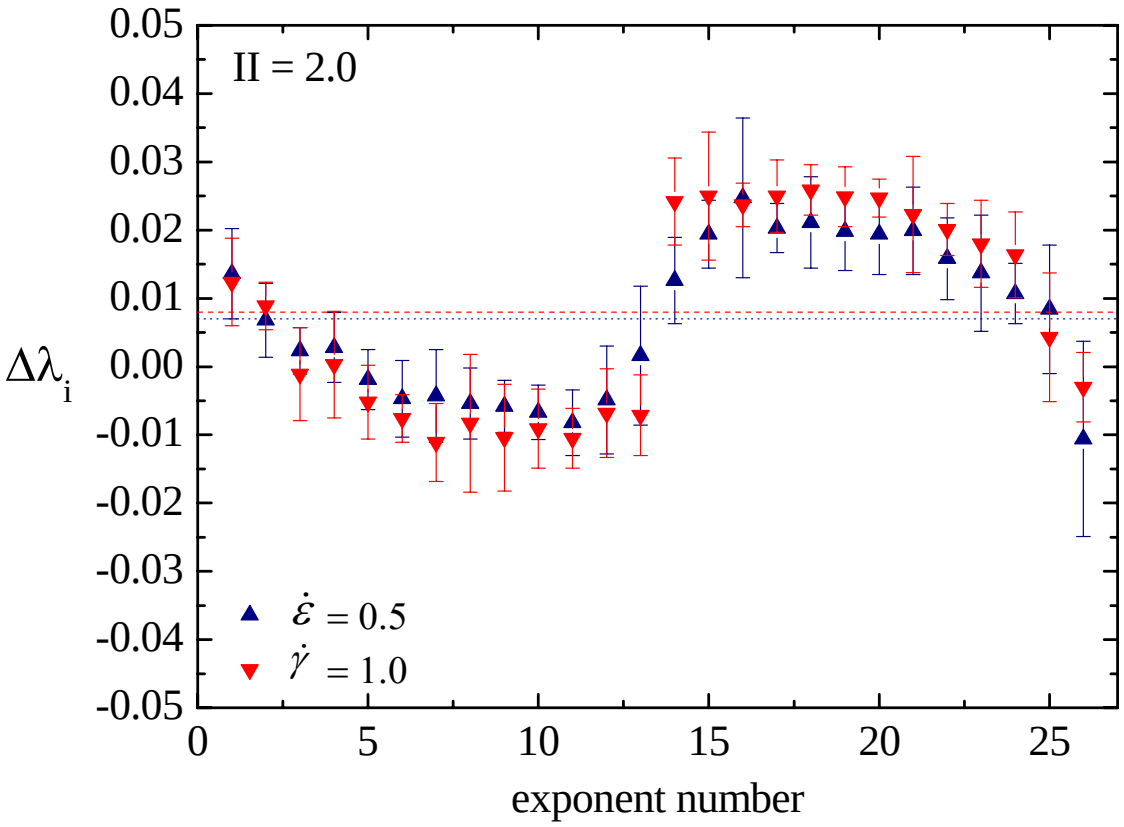

Fig. 3. Frascoli *et al*

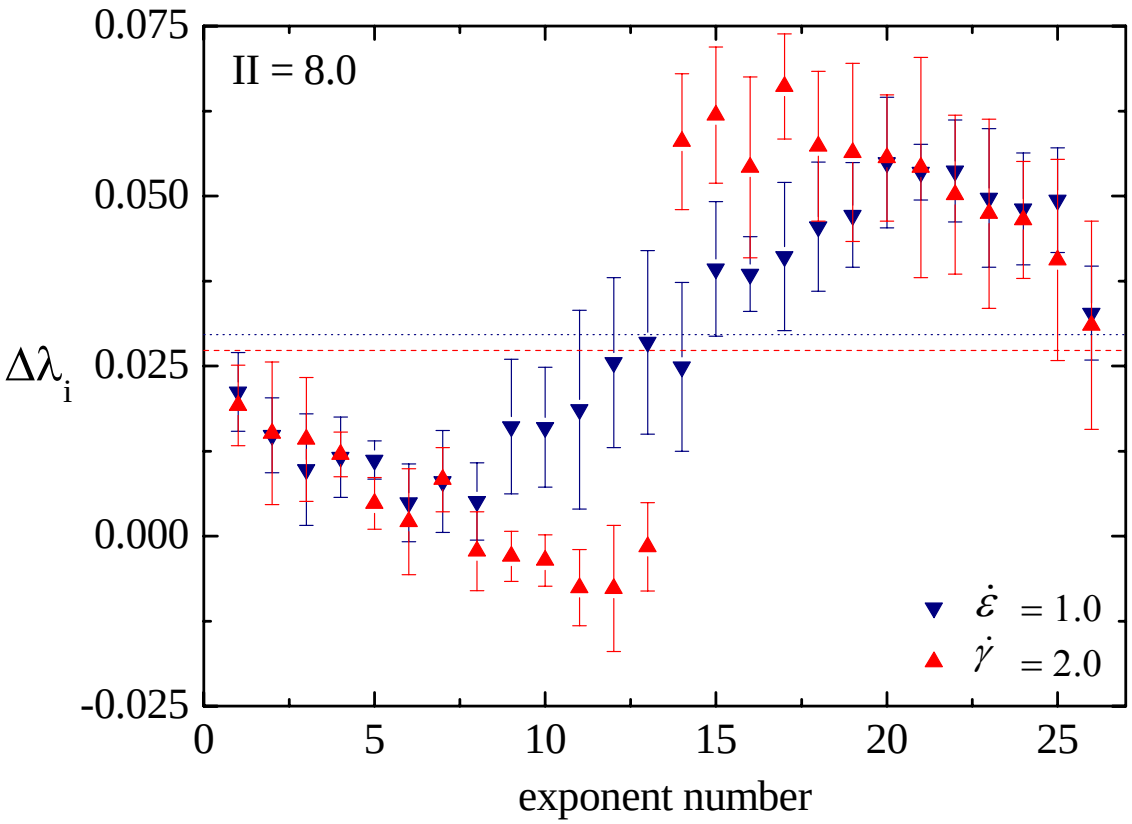

Table captions.

Table 1. Summary of results for *NpT* simulation for 8 particles at equilibrium and under PSF and PEF, using a target pressure equal to the average pressure arising from equivalent *NVT* simulations in [7]. p_0 is the target pressure, p is the average pressure and V indicates the average volume of the simulation cell. $\lambda_{\max}$ and $\lambda_{\min}$ are the maximum and minimum Lyapunov exponents, $\sum_{i;\lambda_i>0} \lambda_i$ is the sum of the positive Lyapunov exponents, max dev is the maximum deviation (Eqs. (15)-(16)) expressed as a percentage of the total sum of the computed Lyapunov exponents, η_{NEMD} is the viscosity calculated with NEMD simulations (Eqs.(10)-(11)), η_{L} is the viscosity calculated with Eqs. (12)-(13), η_{CPR} is the viscosity calculated using CPR for the maximum and minimum Lyapunov exponents and D_{KY} is the Kaplan-Yorke dimension from Eq. (14). Where relevant, uncertainties are next to the computed averages, expressed as twice the standard error from 3 independent runs. *NVT* simulations in [7] have been performed at a constant $V = 26.67$.

Table 2. Comparison of values for conjugate pairing and phase space compression factors between different ensembles. $\Delta\Lambda$ and $(2N\text{-}1)\Delta\alpha$ represent the left and right hand side of Eq. (17), respectively. Uncertainties are next to the relevant quantities, expressed as twice the standard error from 3 independent runs.

Table 3. Thermodynamical properties and values of the extra couple of Lyapunov exponents associated with the NH degrees of freedom, under different *NpT* state points.

Label A indicates simulations at the same target pressure of previous *NVT* results, whereas B, C and D correspond to different state points. All data are collated from 3 independent runs except for set D, where 10 runs have been executed, and uncertainties expressed as twice the standard error are next to the relevant quantities.

Table 1. Frascoli *et al*.

Type	rate	α		λ_{max}		λ_{min}		$\sum_{i;\lambda_i>0} \lambda_i$		max dev (%)	p_0	V		p		η_{NEMD}		η_L		D_{KY}	
Equil		/	/	1.786	0.003	-1.789	0.003	14.84	0.01	/	0.4481	27.89	0.05	0.4475	0.0003	/	/	/	/	29.0	/
PSF	1.0	0.391	0.002	1.763	0.004	-2.151	0.003	13.42	0.03	0.017	0.4792	27.82	0.02	0.4783	0.0004	0.197	0.001	0.221	0.001	26.4	0.1
	2.0	1.180	0.008	1.804	0.003	-2.977	0.012	12.08	0.02	-0.039	0.5473	27.56	0.05	0.5480	0.0015	0.150	0.001	0.166	0.001	22.9	0.1
PEF	0.5	0.426	0.004	1.809	0.004	-2.240	0.011	15.63	0.01	-0.024	0.4797	27.80	0.07	0.4788	0.0003	0.215	0.001	0.239	0.003	26.2	0.1
	1.0	1.295	0.004	1.931	0.003	-3.217	0.003	16.87	0.04	-0.023	0.5366	27.54	0.04	0.5367	0.0009	0.165	0.001	0.182	0.002	23.0	0.1

Table 2. Frascoli *et al*.

Type	rate	$(CPR)^{NVT}$		$(CPR)^{NpT}$		Λ^{NpT}		Λ^{NVT}		$\Delta\Lambda$		$(2N-1)\Delta\alpha$	
PSF	1.0	-0.39	0.01	-0.38	0.01	-6.08	0.04	-6.32	0.07	0.24	0.11	0.25	0.06
	2.0	-1.21	0.06	-1.15	0.06	-18.23	0.13	-19.13	0.11	0.90	0.23	0.89	0.13
PEF	0.5	-0.43	0.01	-0.41	0.01	-6.63	0.05	-6.86	0.07	0.22	0.12	0.24	0.07
	1.0	-1.31	0.05	-1.26	0.05	-20.09	0.07	-21.04	0.09	0.95	0.16	0.98	0.11

Table 3. Frascoli *et al*.

Label	Type	rate	ρ	T	max dev (%)	p_0	p		Δp (%)	λ_+		λ_-	
A	Equil	0.0	0.3	1.0	/	0.4481	0.4475	0.0003	-0.12	0.020	0.001	-0.021	0.001
A	PSF	1.0	0.3	1.0	0.017	0.4792	0.4783	0.0004	-0.18	0.021	0.001	-0.023	0.001
A		2.0	0.3	1.0	-0.039	0.5473	0.5480	0.0015	0.12	0.028	0.001	-0.017	0.001
B		1.0	0.4	1.0	-0.051	0.4792	0.5148	0.0002	7.42	0.022	0.001	-0.022	0.001
B		2.0	0.4	1.0	-0.032	0.5473	0.6147	0.0010	12.32	0.052	0.004	-0.017	0.001
C		1.0	0.4	1.0	-0.102	0.8000	0.8004	0.0010	0.05	0.023	0.001	-0.023	0.001
C		2.0	0.4	1.0	-0.058	1.0000	1.0016	0.0024	0.16	0.023	0.001	-0.035	0.002
D		1.0	0.3	1.5	-0.053	0.5750	0.5881	0.0009	2.27	0.019	0.001	0.021	0.001
D		2.0	0.3	1.5	-0.064	0.6568	0.6592	0.0003	0.37	0.050	0.002	-0.053	0.003
A	PEF	0.5	0.3	1.0	-0.024	0.4797	0.4788	0.0003	-0.20	0.022	0.001	-0.022	0.001
A		1.0	0.3	1.0	-0.023	0.5366	0.5367	0.0009	0.01	0.023	0.001	-0.024	0.001
D		0.5	0.3	1.5	-0.103	0.5756	0.5892	0.0005	2.35	0.019	0.001	-0.021	0.001
D		1.0	0.3	1.5	-0.066	0.6492	0.6523	0.0008	0.48	0.021	0.001	-0.022	0.001